Chapter 3

Optical, Radio and X-ray Observations of GRB Afterglows

Abstract

In this chapter we describe the telescopes, their specifications, the filter systems used with them and the detectors used for the observations of the GRB afterglows. The entire optical photometry of the observed GRB fields was done using the Charge Coupled Devices (CCDs) mounted on Sampurnanand Telescope and Himalayan Chandra Telescope. We also describe in detail the procedure used for cleaning and analysing the images and for deriving photometric magnitudes of the stars and of the GRB afterglows. Radio observations of the afterglows were performed using the Giant Metrewave Radio Telescope. We discuss the observational strategy and techniques of radio data reduction. We used the x-ray afterglow observations conducted by the *Swift-XRT*. We describe the data analysis methods we have followed for reducing the x-ray afterglow data.

3.1 Introduction

During the course of this thesis we have observed and analysed the afterglows of a few GRBs in radio and optical. We used the x-ray observations of the afterglows conducted by *Swift* and analysed them for the purpose of modeling. In this chapter we describe the various telescopes we have used for these observations along with the techniques we have followed for their analysis.

We discuss the optical observations in § 3.2, radio observations in § 3.3 and the x-ray observations in § 3.4. Optical telescopes which we have used are discussed in detail in § 3.2.1 which is followed by the methods of data reduction and analysis of optical observations in § 3.2.2. The principles and techniques of radio interferometric observations and hence of data reduction are very different from those of optical or x-ray observations. We have briefly described the principle of radio interferometry and aperture synthesis, respectively in sections § 3.3 and § 3.3. We have used Giant Metrewave Radio Telescope (GMRT) extensively for radio observations of GRB afterglows. We briefly describe the telescope in § 3.3.1. The data reduction of radio observation is described in § 3.3.2. For the X-ray observations of GRB afterglows, we made use of the observations conducted by X-ray Telescope (XRT) aboard satellite *Swift*. The XRT is described briefly in § 3.4.1 and x-ray data reduction methods in § 3.4.2. We have converted all the observations in optical and radio into Jansky units for comparison and model fitting. The light curves obtained from x-ray data reduction are in *counts* s^{-1} units, instead. So finally, in § 3.4.2.4 we describe the method we followed to convert the x-ray fluxes from *counts* s^{-1} to Jansky units.

3.2 Optical Observations

While the Earth's atmosphere is relatively transparent in this portion of the electromagnetic spectrum, optical observations strongly depend on the seeing conditions which can severely affect the resolution and image quality of the instrument. The presence of a bright moon near the field of interest can also cause trouble with significant background brightness which can restrict the observations from detecting very faint objects. For observation purposes, the optimal location for an optical telescope is undoubtedly in outer space.

Apart from the above mentioned problems, ground based optical observations have to worry about the atmospheric effects on the brightness of the stars also. The atmosphere scatters starlight leading to diminished brightness of the stars. Similarly, the interstellar medium also diminishes the stellar brightness as the starlight propagates through it. To estimate the correct brightness of a star one has to properly understand these various effects and account for it while calculating stellar brightness.

In this section, we will briefly discuss these aspects of the optical observations. We will start with description of the telescopes which we used for afterglow observations.

3.2.1 Telescopes

The Sampurnanand Telescope (ST)[1] and the Himalayan Chandra Telescope (HCT) [2] operated by the Aryabhatta Research Institute of Observational Sciences (ARIES, Naini Tal) and the Indian Institute of Astrophysics (IIA, Bangalore), respectively, are the two telescopes which have played a major role in India's contribution towards

[1] http://aries.ernet.in/

[2] http://www.iiap.res.in/iao_telescope.htm

the observations of optical and near infra-red (IR) afterglows of GRBs. We have used ST and HCT extensively for the observations of the GRB afterglows presented in this thesis. The important parameters of the telescopes are presented in the Table 3.1 below.

3.2.2 Data Reduction and Analysis

The raw images of the sky can not directly be used to extract the stellar magnitudes. It is important to know the detector behaviour during the observations and correct for it before determining what it has detected. The characteristics of the detector system (Telescope mirror + filters + CCD) can change from one night to another night. The detector system not only detects the objects of our interest but also various other 'contaminants' (mostly cosmic rays). The contribution from these contaminants have to be taken out of the images and the images have to be calibrated for the CCD response before they can be used for extracting stellar magnitudes. Even the magnitudes so extracted may not be useful for extracting important scientific information simply because atmospheric conditions does affect the measurements. So the effect of the atmosphere has to be taken into account. And ultimately, the magnitudes thus corrected for the local atmospheric effects by two observers from two different places in the world will still not agree with each other because they have used different instruments for the observations. These final magnitudes then have to be calibrated to global standards. Thus, from raw images to the final product is a lengthy procedure with various techniques of optical data reduction used on the way. Below, we briefly summarize the entire procedure, from raw images to calibration to the standard magnitude system in three stages : [1.] Cleaning, [2.] Analysing and [3.] Standardising of optical images.

	Sampurnanand Telescope (ST)	**Himalayan Chandra Telescope (HCT)**
Size of Primary Mirror (meter)	1.04	2.01
	f/13, RC, 15.5″/mm	f/9, RC, 11.5″/mm
Longitude	79° 29′ *E*	78° 58′ *E*
Latitude	29° 22′ *N*	32° 46′ *N*
Altitude (meter)	~ 1955	~ 4500
Filters	Johnson *UBV* & Cousins *RI*	Bessel *UBVRI*
	Filter/$\lambda_c(\mu$m)/BW(μm)	Filter/$\lambda_c(\mu$m)/BW(μm)
	U/0.36/0.06	U/0.35/0.05
	B/0.44/0.09	B/0.44/0.09
	V/0.55/0.09	V/0.55/0.08
	R/0.64/0.16	R/0.65/0.15
	I/0.80/0.15	I/0.79/0.11
Detector	TK2048E CCD	E2V CCD
Temperature (°C)	-120	-110
Size (pixel^2)	2048 x 2048	2048 x 4096
Pixel Size (μm^2)	24 x 24	15 x 15
Gain (e^-/ADU)	10	1.22
Readout Noise	5.3 e^- (130 KHz)	4.8 e^- (130 KHz)

Table 3.1: **Optical Telescopes :** System parameters of the telescopes, filters and detectors used for the observations of optical afterglows.

3.2.2.1 Cleaning

The process of *cleaning* the CCD images include bias-subtraction, flat fielding and removal of cosmic ray events from the images. The *raw frames* i.e. the images of the sky as obtained by the CCD are processed using a set of *bias frames* (i.e. a zero second exposure frame) and a set of *flat frames* (i.e. a few seconds exposure frames) obtained using the same filter as that of the *raw frames* .

The *bias frames* are zero seconds exposure frames which consists only of CCD readout. The *bias frames* thus contains pixel by pixel information about the noise level due to the CCD electronics. To remove this noise offset from all the *raw frames* a set of *bias frames* is combined into one standard bias frame using an IRAF task ZEROCOMBINE which is then subtracted from all of the *raw frames* . Generally a set of five or more *bias frames* is used for statistically significant sampling of the electronics noise and the variation.

Even then the resultant bias-subtracted frames do not have uniform response across the CCD because each pixel of the CCD acts as an independent detector and can have a significantly different response from the rest of the pixels. To measure response of the individual pixels the CCD is illuminated uniformly by exposing it to a patch of the sky which is not very bright but uniformly illuminated. Under such exposure, the images of the sky are obtained under different filters. These are called the *flat frames* . A set of *flat frames* under a given filter are combined using an IRAF task FLATCOMBINE to get average *flat frames* for different filters. The bias-subtracted images are then divided using these average *flat frames* .

The bias-subtracted and flat-fielded images thus obtained contain a few bright specks which are distinct from the stars in their intensity profile. Unlike the stars which have Gaussian-like profiles (a peak and broad wings), the bright specks have sharply rising and falling profile. These bright specks are cosmic ray events.

An IRAF task COSMICRAYS is used to remove the cosmic ray events from the flat-fielded frame.

The images thus obtained are referred to as 'clean' images and are used for further analysis to obtain stellar magnitudes. First it is important to note that the GRB afterglows are generally faint and sometimes may not be seen clearly in the images. This is usually because the exposure time of the frame was not long enough to detect the source of interest (GRB afterglow in our case). Increasing the exposure time is an obvious solution. However, increasing the exposure time may not always be practical due to a variety of reasons. Even in such situations it is possible to increase the 'effective exposure time' of the images post-observations by stacking the images of shorter exposure times thus increasing the significance level of the detection of the source of interest.Quantitatively, *signal to noise ratio* or S/N is the quantity which tell us the significance of the signal (S) over the underlying noise (N). For the faint signals, the statistical noise fluctuation is represented by the Poisson distribution where $S \propto counts$ and $N \propto \sqrt{counts}$. Thus $S/N \propto \sqrt{counts}$. Increasing the number of counts, either by increasing the exposure time when possible or by combining images of different exposure times post-observations, would increase the S/N ratio making the source of interest visible. It is necessary to align the different images obtained under the same filter before combining. An IRAF task IMALIGN is used to align the images. The aligned images are then combined using a task IMCOMBINE provided by IRAF.

3.2.2.2 Analysing

The clean, and if required combined, images are analysed using simple analytical or numerical methods for the purpose of identifying stars and measuring their brightness. We have used DAOPHOT-II extensively for analysing the clean CCD images.

Detecting stars in a clean image

DAOPHOT provides a task FIND for 'finding' or identifying stars. Unlike extended objects like galaxies, the stellar brightness distribution is supposed to have a Gaussian or a similar profile which peaks at the center and falls off rapidly on either sides. This property is used by the task FIND for identifying stars in a given CCD frame.

FIND performs a pixel by pixel search for brightness enhancements and then fits a Gaussian profile to such enhancements. The location where the fit finds large, positive value lies near center of the star. FIND reports the positions of stars identified in this way in the CCD pixel-based X, Y coordinates.

Photometry

Photometry of stars implies assigning quantitative measure to the brightness of the detected stars. This is performed by using a task PHOT provided by DAOPHOT. There are two popular procedures which are routinely followed for doing the photometry in DAOPHOT : 1) Aperture Photometry and 2) Profile Fitting Photometry.

Aperture Photometry

Aperture photometry is the simplest of the two. It calculates and sums the brightness of a star within a series of concentric annuli (referred to as the apertures and hence the name of the method) with increasing radii centred on the star. Far away from the centre of the star, where the contribution due to the star's brightness is expected to be small or zero, another annulus is used to estimate the brightness due to the background. The area-weighted background is then subtracted from the stellar brightness. This final number is then converted into magnitude.

The obvious advantage of this method is that it is simple. It works fine when the imaged field is not crowded. In a crowded field optimizing apertures is difficult as they might merge with the apertures of nearby stars. Also, in such a field

proper estimate of the background is difficult. The alternative technique of Profile Fitting Photometry comes to our rescue to some extent in such situations.

Profile Fitting Photometry

This technique assumes or estimates functional form of the point spread function (PSF) of a few observed bright stars and for the rest scales it according to the peak brightness of individual stars. This technique is based on the simplifying assumption that under identical observing conditions (atmospheric and technological) all the stars would have identical brightness profiles and would differ from one another only by scaling of the peak intensity. The PSF is approximated by a number of mathematical functions, the most common among them are :

$$\begin{aligned} G(r,a) &\propto exp(-\frac{r^2}{2\ a^2}) && \text{Gaussian} \\ L(r,a,b) &\propto \frac{1}{1+(r^2/a^2)^b} && \text{modified Lorentzian} \\ M(r,a,b) &\propto \frac{1}{(1+r^2/a^2)^b} && \text{Moffat} \end{aligned} \tag{3.1}$$

where r is the distance from the centre and a & b are the parameters to be fitted (Stetson, 1987). Approximating the PSF using such mathematical functions yields an analytical PSF. Another way of estimating PSFs is numerical where the functional form of the PSF is approximated using a few bright stars in the field. The advantage with the analytical PSFs is that they can be integrated analytically over the entire stellar profile to get the total brightness. But the disadvantage is that they can only be an approximation as the real stellar profile could be different from such functional forms. The advantage with the numerical PSFs is that they could be very close representation of the real stellar profile. But the disadvantage is that they are expensive computationally. Better results could be obtained by combining best of the two methods. The task ALLSTAR provided by DAOPHOT determines PSFs by a combination of both, the analytical and the numerical methods.

ALLSTAR uses about 20 well isolated bright stars to determine the PSF and this applies to all the stars in the field. As an output, ALLSTAR provides positions and magnitudes of the stars with errors on the magnitudes, sky brightness and χ^2 values.

3.2.2.3 Standardising

The magnitudes of the stars thus estimated are called as the instrumental magnitudes. These are specific to the observing conditions (atmospheric and technological) e.g. the magnitudes of a star determined today and tomorrow under different observing conditions could turn out to be different or the magnitude of the same star as estimated by two different telescopes could be different. To be able to compare results from different telescopes and under different observing conditions astronomers have come up with a standard magnitude system. In this system a number of stars are identified as primary standards. The observers have to bring their own measurements to a similar level of these primary standards to be able to compare them with the measurements of others. This process is called as the *Standardisation*. We will briefly describe here the steps for achieving standardisation.

- **Observations :** It requires observing the standard Landolt fields of stars (Landolt, 1992) along with the field of interest. The instrumental magnitudes of all the stars in both the fields are then estimated.

- **Atmospheric Extinction :** Stellar light is absorbed and scattered while passing through the Earth's atmosphere towards the Earth based observer and hence gets extincted. This effect is called Extinction. The atmospheric extinction depends primarily on the zenith distance (Z) and the wavelength of the radiation. During the observations the zenith distance of an object keeps changing

and as a result, the amount of light extincted. To take this into account, atmospheric extinction has to be estimated during the observations. For this, airmass (X) is calculated using the following equation :

$$X = sec(Z) - 0.0018167[sec(Z) - 1] - 0.002875[sec(Z) - 1]^2 - 0.000803[sec(Z) - 1]^3$$

$$cos(Z) = sin(\phi)sin(\delta) + cos(\phi)cos(\delta)cos(H)$$

where ϕ is the latitude of the observer, δ is the declination of the source and H is the hour angle of the source.

- **Transformation Equations :** We will list the required transformation equations here directly. The details are in the standard texts e.g. Henden and Kaitchuck (1982). The required transformation equations are

$$\begin{aligned} u_i &= U + u_0 + u_1(U - B) + u_2 X \\ b_i &= B + b_0 + b_1(B - V) + b_2 X \\ v_i &= V + v_0 + v_1(V - R) + v_2 X \\ r_i &= R + r_0 + r_1(R - I) + r_2 X \\ i_i &= I + i_0 + i_1(V - I) + i_2 X \end{aligned}$$

The quantities with subscript '0' are the zero points. The quantities $(u_1, b_1, v_1, r_1, i_1)$ are the color coefficients and $(u_2, b_2, v_2, r_2, i_2)$ are the atmospheric extinction coefficients for filters (U, B, V, R, I), respectively. X is the airmass and (U, B, V, R, I) are the standard magnitudes. Corresponding instrumental magnitudes are $(u_i, b_i, v_i, r_i, i_i)$. The second order color correction terms are ignored as they are usually small compared to other errors present in the measurements of the magnitudes.

- **Coefficients of Atmospheric Extinction :** As can be seen from the above equations, the instrumental magnitudes have a linear dependence on the airmass

(X). To determine the co-efficient of atmospheric extinction one needs magnitudes of stars through different airmass i.e. at different elevations above the horizon. By observing the stars in a given field at various times during the observation one can determine the magnitudes of the stars through different airmasses which can be further used to determine the coefficients of atmospheric extinction. This procedure is repeated for all the required filters to determine respective co-efficients.

- **Coefficients of Transformation :** By using observations of a large number of stars in the field of view one can determine the rest of the transformation coefficients. For this purpose we have used tasks COLLECT and CCDSTD. The transformation coefficients can be applied along with the known magnitudes of standard stars to generate a set of secondary stars in the field of view of the source of interest. The tasks CCDAVE and FINAL can be used for this purpose.

3.3 Radio Observations

The imaging at radio wavelengths is, unlike at optical and x-ray wavelengths, based on the principle of Aperture Synthesis and Interferometry (Ryle and Hewish, 1960). The sensitivity of a telescope is directly proportional to its collecting area. The angular resolution of a telescope is diffraction limited and is given by the Rayleigh criterion $\theta \sim \lambda$/D where λ is the wavelength of the observations and D is the diameter of the telescope. In optical and x-ray observations, since λ is small the desired resolution can be obtained with a small sized mirror. To achieve a resolution comparable to the resolution of a small size optical telescope would require a gigantic radio telescope (nearly 10^5 times the size of the optical telescope !) which is expensive and

unfeasible. As a result radio astronomers use the interferometric technique, where instead of a single giant dish of several tens of kilometers, one works with several dishes of smaller size spread over a few tens of kilometers. This acts coherently as a big telescope of a few tens of kilometer diameter, albeit not covering it fully.

Interferometry

Radio interferometry with a two antenna interferometer is similar to the double slit experiment. Consider an astronomical phenomenon on the celestial sphere of radius **R** leading to a time varying electromagnetic signal **E(R)** which will eventually arrive at the observer at **r**. The field at the observer **E(r)** is related to the field at the source $\mathbf{E}(\mathbf{R}, t)$ as follows

$$\mathbf{E}(\mathbf{r}) = \int \mathbf{E}(\mathbf{R}, t) \frac{e^{2\pi i \nu |\mathbf{R}-\mathbf{r}|/c}}{\mathbf{R}-\mathbf{r}} d\Omega \tag{3.2}$$

where $d\Omega$ is the surface area element on the surface of the celestial sphere of radius **R**. The fundamental property of the radio waves received from astronomical sources is that they are 'stochastic' i.e. the electric field at the observer due to an astronomical source can be treated as a random process. The commonly used statistic for a random process is the correlation function. Using this property one can define a quantity called 'Complex Visibility'

$$\mathrm{V}(\mathbf{r_1}, \mathbf{r_2}) = < \mathbf{E}(\mathbf{r_1}, \mathbf{r_2}) \mathbf{E}^*(\mathbf{r_1}, \mathbf{r_2}) > \tag{3.3}$$

which is averaged in time for the measurements of the signal at locations $\mathbf{r_1}$ and $\mathbf{r_2}$. In radio astronomy, it is customary to measure distances in the observing plane in units of the wavelength λ and to define 'baseline co-ordinates' (u, v, w) such that $\mathrm{u} = (x_2 - x_1)/\lambda$, $\mathrm{v} = (y_2 - y_1)/\lambda$ and $\mathrm{w} = (z_2 - z_1)/\lambda$. The van Cittert-Zernike theorem relates the Visibility function $V(\mathbf{u}, \mathbf{v}, \mathbf{w})$ to the intensity distribution of the incoming radiation, $\mathrm{I}(l,m)$, where l and m are the direction cosines on the sky

in 'uvw' co-ordinate system. It can be shown that $(l^2 + m^2 + n^2) = 1$ and that $d\Omega = dl\ dm/\sqrt{1 - l^2 - m^2}$. With these definitions Equation 3.3 can be rewritten as

$$V(u,v,w) = \int\int I(l,m)A(l,m)e^{2\pi i(ul+vm+w\sqrt{1-l^2-m^2}-1)}\frac{dldm}{\sqrt{1-l^2-m^2}} \qquad (3.4)$$

where $A(l,m)$ is the normalised primary beam pattern. The above equation is a Fourier Transform relation between the visibility function and the modified intensity $I'(l,m) = I(l,m)/\sqrt{1-l^2-m^2}$. The Inverse Fourier transform of this visibility leads to the estimation of the source intensity distribution.

Aperture Synthesis

From the previous section it is clear that to 'map' the intensity distribution of the source we need to have its Fourier components i.e. visibility measurements. Moreover, if the source is not varying, at least for the purpose of observations, then it not necessary to measure all the Fourier components simultaneously. This is a great simplification at the instrumental requirements for effectively one can measure all the Fourier components by using only two antennas, by physically moving one antenna with respect to the other from place to place. This method of gradually building all the Fourier components and using them to image the source is called 'Aperture Synthesis'. In practice, instead of physically moving antennas from place to place, one uses the rotation of the earth to sample the (u,v) plane and the visibility function quite rapidly.

3.3.1 Giant Metrewave Radio Telescope (GMRT)

GMRT is an interferometric array which uses the principle of aperture synthesis invented by Ryle and Hewish (1960). The GMRT consists of 30 fully steerable dishes, each of diameter 45 m, and has been designed to operate at a range of frequencies from 50 MHz to 1450 MHz. A description of the GMRT is given by

Swarup (1990). The GMRT is located at a site (longitude = 74°03′ E, latitutde = 19°06′ N, altitude = 650 m above mean sea level) ~ 80 km north of Pune, India. The GMRT antennas have a very low wind loading and very low total weight (~ 80 tonnes) thanks to the novel technique called SMART - Stretch Mesh Attached to Rope Trusses. A light thin wire mesh of 0.55 mm diameter with a varying grid size : 10×10 square mm in the inner 1/3 area of the dish, 15×15 square mm in the middle 1/3 area of the dish, 20×20 square mm in the outer 1/3 area of the dish stretched over rope trusses forms the reflecting surface of the dish. The important system parameters for the GMRT are listed in Table 3.2.

The configuration of GMRT array is optimized to meet the requirement of high angular resolution at low frequencies as well as imaging diffuse extended radio emission. This optimization is achieved using a hybrid configuration of the array : with 14 of the antennas randomly distributed in a region of about 1×1 square km in the central region, called 'Central Square', and the remaining 16 antennas being spread out in a roughly 'Y' shaped configuration with the length of each arm of the 'Y' being ~ 14 km. See Figure 3.1. The distribution of the antennas in the central square was deliberately randomized to avoid grating lobes. The central square antennas provide a large number of short baselines, shortest being ~ 100 m. This is useful for imaging extended sources whose visibilities are concentrated near the origin of the *uv* plane. The arm antennas with longest baseline ~ 14 km, provide high angular resolution. A single GMRT observation hence yields information on a variety of angular scales.

3.3.1.1 Observations with GMRT : A strategy

The antenna gains (which are complex) can vary with time and frequency. Proper tracking of these temporal and spectral variations in the gain of each antenna is

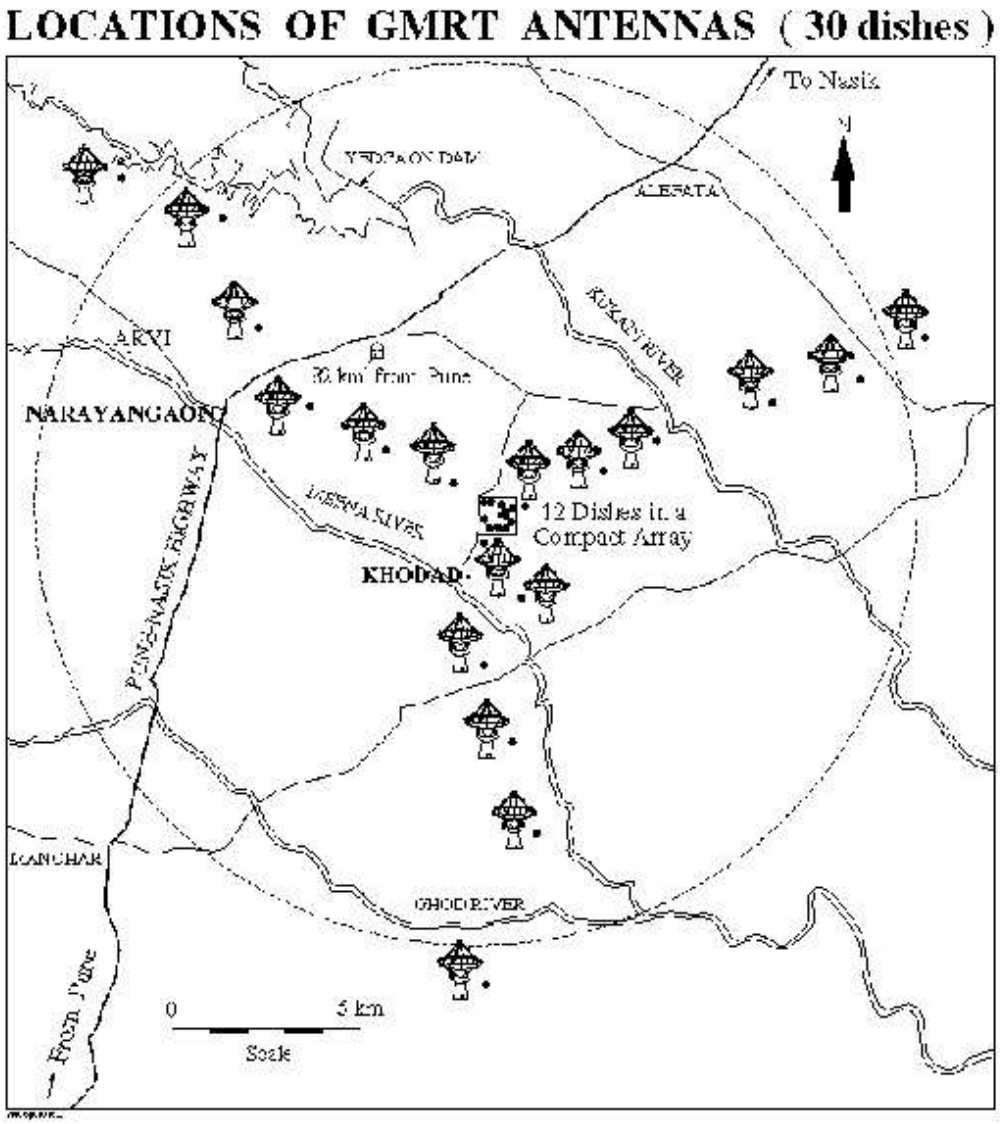

Figure 3.1: **GMRT antenna array in 'Y' shape :** The antennas of GMRT are fixed at their positions, unlike VLA antennas which are all mounted on rails and can be moved when required. The 'central square' consists of 14 antennas and the rest 16 antennas are spread in the three arms of the 'Y'. The logest baseline provided by GMRT is ∼ 14 km while the shortest is ∼ 100 m. The whole configuration effectively works as a single antenna dish of 25 km diameter, albeit with non-uniform sampling over the surface.

System Properties		Frequencies in MHz				
	50	153	233	327	610	1420
Primary Beam (degrees)	planned	3.8	2.5	1.8	0.9	$0.4 \times (1400/f)$
Synthesised Beam						
Full array (arcsec)	planned	20	13	9	5	2
Central Square(arcmin)	planned	7.0	4.5	3.2	1.7	0.7
System Temperature (K)	planned	482	177	108	92	76
Gain of an antenna(K/Jy)	planned	0.33	0.33	0.32	0.32	0.22
rms noise† in image(μJy)	planned	46	17	10	9	13

Table 3.2: **System parameters of the GMRT :** † For assumed bandwidth of 16 MHz, integration of 10 hrs and natural weighting (theoretical)

important to get meaningful results out of the radio interferometric observations. Creating an observation strategy, keeping in mind the requirements of antenna gain calibration, is a first step for such observations. The complex gain of an antenna can be specified using an amplitude and a phase. Therefore, one needs two types of calibrators, a flux calibrator and a phase calibrator, to track the amplitude and phase variations of the gain. Keeping this in mind during the observations, the source of interest (Target) is observed along with the Flux calibrator (Flux Cal) and the phase calibrator (PhaseCal) in a sequence : **FluxCal - PhaseCal - Target - PhaseCal - Target -..... - Target - PhaseCal - FluxCal** The gain variations across the frequency bandpass are corrected using bandpass calibration which we shall discuss briefly later.

3.3.1.2 Flux Calibration

The amplitude of the visibility function of a single point source is proportional to the flux density of the source. Therefore, visibility measurements of a point source of known flux density can be used to estimate the scaling between the flux densities

Source	A	B	C
3C48	2.345	0.071	-0.138
3C147	1.766	0.447	-0.184
3C286	1.480	0.292	-0.124

Table 3.3: **Flux Calibrators :** Parameters A, B ad C mentioned in Equation 3.5

of the point source (calibrator) and the source of interest which can then be applied to the rest of the observations. A flux calibrator (which should be a point source) of known flux density is used for this purpose and is observed at the beginning and end of the observation. The standard flux density calibrators are listed in Table 3.3. According to the formulation given by Baars et al. (1977), the flux density F (in Jy) of the flux calibrators at a frequency ν (in MHz) is given as

$$log(F) = A + B \times log(\nu) + C \times (log(\nu))^2 \tag{3.5}$$

The constants A, B and C are listed in Table 3.3.

3.3.1.3 Phase Calibration

The ionosphere affects the direction as well as the phase of the signal arriving at antenna. Moreover, the Earth's ionosphere also shows density fluctuations on a large range of length and times scales. The typical angular scale of these fluctuations being a few degrees. The phase variations in the signals received at the antennas result in variation in the estimated antenna gains. To correct for these the phase calibrator is observed for a few minutes repeatedly at an interval of about 45 minutes during the observing run. Since these phase variations are caused due to atmospheric effects over an angular scale in the sky which is of a few degrees, the phase calibrator is chosen such that it is within a few degrees from the target source.

Source	Frequency (MHz)	Date (UT)	ΔT (days)	Flux (mJy)	Reference
†GRB 030329	1280	–	–	Detection	a
†GRB 030329	610	–	–	Detection	a
†GRB 030329	325	–	–	< 0.5 (1 σ)	a
GRB 050408	1280	2005, Apr. 21 & 22	13	< 0.45 (3 σ)	b
GRB 050416A	1280	2005, Apr. 25.83	9.4	< 0.094(2 σ)	c
XRF 050509c	1280	2005, Jul. 6.56	57.6	< 0.22 (2 σ)	d
		2005, Aug 4.48	86.5	< 0.12 (2 σ)	d
GRB 060218	1280	2006, Feb. 21.65	3.5	< 0.3 (3 σ)	e, f

Table 3.4: **Radio Afterglows :** A list of GRB afterglows observed (detections and non-detection) using GMRT. [References : a = van der Horst et al. (2007); b = de Ugarte Postigo et al. (2007); c = Ishwara-Chandra et al. (2005); d = Kamble et al. (2005), e = Kamble et al. (2006b); f = Kamble et al. (2006a).] †The afterglow of GRB 030329 was observed by GMRT on several occasions. It was detected at 1280 MHz and 610 MHz while at 325 MHz we could establish only upper limits. A complete list of observations of GRB 030329 radio afterglow can be found in van der Horst et al. (2007).

3.3.1.4 Bandpass Calibration

The antenna gains vary across the frequency band of observation mainly because of instrumental errors and at some times due to external Radio Frequency Interference (RFI). Hence, calibration of the bandpass is necessary. A strong flux calibrator (providing good signal to noise ratio) can be used for bandpass calibration as well. The average gain per channel can be used to look for the relative variations of the antenna gain in the frequency band of observation. Severely affected channels thus detected could be omitted before interpolating and applying the antenna gains to the target source.

3.3.1.5 Issues

There are a few other complications with the radio observations which one has to be aware of and should take care of while analysing the data. To mention a few of these issues : the antenna gain variation with the source elevation, phase fluctuations due to ionosphere, image smearing due to finite bandwidth and finite time of integration, zero spacing problem and non-co-planarity of the baselines. Below we discuss briefly only a few of these issues which are relevent particularly for our observations.

1. **Ionospheric Phase Fluctuations :** Phase fluctuations due to ionosphere is a frequency dependent effect and low frequency data is often significantly affected by these fluctuations. To make the matter worse, the Sun and solar activity directly affect the Earth's ionosphere which affects the phase measurements during the radio observations. These phase fluctuations affect the sensitivity of the observations and hence the estimates of the flux values. It is important to calibrate these phase fluctuations before using the measured visibilities for mapping. Periodic observations of the phase calibrator along with the technique of 'self calibration' can provide a remedy to this problem so far as the phase fluctuations are small. This technique is discussed in section 3.3.2.4.

2. **Bandwidth smearing :** The manifestation of the effect of band-width smearing in a radio map is the **radial distortion** of the sources i.e. the sources appear elongated towards the phase centre of the map. For continuum observations, the visibility data integrated over the band-width $\Delta\nu$ is treated as if the observations were made at a single frequency ν_0 which is the central frequency of the band. As a result, the u and v co-ordinates and the values of the visibilities are correct only for ν_0. It follows from the definition of the (u,v) co-ordinates that the true co-ordinates are related to the recorded co-ordinates and the

frequency as $(u, v) = (u_\nu \nu_0/\nu, v_\nu \nu_0/\nu)$. The relation between the brightness distribution and the visibility changes accordingly. The effect of the co-ordinate scaling is to smear a point at position (l, m) into a line of length

$$L = (\Delta\nu/\nu_0)\sqrt{(l^2 + m^2)} \tag{3.6}$$

in the radial direction. The larger the fractional bandwidth, more is the distortion it causes. This reduces the amplitude of the visibility and affects the final flux estimates significantly. The remedy is, as Equation 3.6 suggests, to split the entire band into several bands of smaller width. This reduces errors in $(u, v) \leftrightarrow \nu_0$ assignment which in turn reduces the effects of bandwidth smearing in the measured visibilities, and in the final flux estimates.

3. **Non-co-planarity of the baselines :** The antenna primary beam is wavelength dependent ($\propto \lambda$). Therefore, at low wavelengths the region of the sky an antenna can 'see' can be approximated by a two dimensional (2-D) plane. But at low frequencies this approximation does not hold good and the plane of the sky that the antenna 'sees' has to be treated as a 3-D plane to avoid distortion free images. We have treated the sky within the primary beam as a set of 2-D planes, for the purpose of initial data reduction, which we later combine properly to recover the full image of the sky. The number of smaller sized 2-D planes (N) required for this purpose is given as $N = \lambda B/D^2$ where λ is the wavelength of observations, B and D are the longest baseline and the diameter of the antenna used, respectively (Taylor et al., 1999).

3.3.2 Data Reduction and Analysis

For data analysis in radio wavebands with GMRT, we used the Astronomical Image Processing System (AIPS) developed by National Radio Astronomy Observatory.

Data is recorded in the lta (long term accumulation) format and is imported to AIPS via the FITS (Flexible Image Transport System) format. GMRT softwares LISTSCAN and GVFITS are used to convert the data in lta format to data in FITS format, which is the AIPS readable format. The imported data in AIPS is in a multi-source visibility database. The data contains multiple tables like source table SU, frequency table FQ, antenna table AN etc.

3.3.2.1 Pre-Processing

The data is loaded into AIPS using task FITLD. Indexing the data is always the first operation to be done on the data which is achieved using the AIPS task INDXR which creates an index (NX) and a calibration (CL) table. The CL table serves as a template of antenna gains for various AIPS calibration programs. It has been found that at the start of each scan the data is invariably not suitable for the purpose of analysis. Therefore, data from the first 0.5 minute of each scan is removed using the task QUACK. The expected flux density of the flux calibrators at the frequency of observations is set using the task SETJY which uses the known spectrum of the source. The information about all the sources, including their flux densities estimated by SETJY are written and maintained in the SU table.

At some times the data may contain defects rendering the data unusable. Such data need be identified and cleaned. The process of removing defective data from the data set is called 'flagging'.

The kind of defects normally observed in the data sets could be of various types e.g. antenna or baselines based – defective antenna or baselines, time based – erratic for a small duration, channel based – defects only in particular channels and a combination of any of the above e.g. a defective baseline only for a small duration of time. It is important to identify the defects clearly and classify within

one of the above types. A wrong identification can result in flagging of even a good quality data which is not desirable, especially when one is looking for faint sources such as afterglows. AIPS provides a variety of tasks to carry out this identification by plotting the data conveniently in various required domains and then for flagging it accordingly. Some of the AIPS tasks which we used for plotting and flagging the data includes : VPLOT, UVPLT, UVFND, UVFLG and TVFLG. All of the above tasks allow plotting of the data in various domains except UVFND and UVFLG which are useful in identifying and flagging of defective data respectively.

3.3.2.2 Calibration

The flux calibrators serves as the primary calibrators for estimating antenna gains which can then be used to calibrate the flux and phases of the phase calibrators which can subsequently be used to calibrate sources of interest. For this reason, flux calibrators are also called as the 'primary calibrators'. The procedure that is routinely followed for calibration is as follows :

- The task CALIB is used to compute complex antenna gains for flux and phase calibrators. This information is written in the corresponding SN tables. One can choose appropriate time resolution over which one wishes to estimate the antenna gains. We have estimated these gains for almost all the available visibilities using a time resolution of 16 seconds. At this stage one can plot the generated SN table using the task SNPLT to check the reliability of the estimated gains. If unsatisfactory, we return to the data flagging step and follow the entire procedure up to this stage again till one is satisfied with the estimated gains.

- The task GETJY is then run to estimate flux density of the phase calibrators using the estimated gains and available data. The flux density of phase cali-

brators thus estimated should then be compared using the calibrator manual provided by VLA [3]. If the results are unsatisfactory then one needs to inspect and flag the bad data further and follow the entire procedure again until the results are satisfactory.

- One can the proceed to bandpass calibration of the data by estimating the bandpasses for all the antennas. This is achieved by using task BPASS which write the estimated bandpasses into a BP table. One can plot the BP tables using a task POSSM. Usually, a few initial and final channels ($\sim$ 5 channels on either sides) do not give satisfactory results and they have to be flagged. If any radio frequency interference (RFI) is present then it can be detected at this stage and the corresponding channels should be flagged.

- The multisource file is then split into a file containing only the source of interest, with all the previous calibrations applied on the uvdata of the source, using the task SPLAT. The resultant calibrated data is then subject to flagging, if required. This data is then ready for the purpose of imaging.

3.3.2.3 Imaging

The task IMAGR, an imaging/Clean task in AIPS is routinely used for creating images using a given uvdata set. It employs a variety of algorithms such as Clark Clean with Schwab/Cotton use of uv-plane subtraction (BGC Clean), and Steer, Dewdeny, and Ito (SDI) Clean.

At low frequencies the effects due to non-co-planarity becomes important. To take these into account IMAGR offers an option of performing 3D imaging. The effect of the non-co-planarity was significant at 610 MHz but not at 1280 MHz. We performed 3D imaging of the source fields for observations done at 610 MHz.

[3] http://www.vla.nrao.edu/astro/calib/manual/csource.html

3.3.2.4 Self Calibration

The procedure of calibration as mentioned above may not be sufficient to produce good quality images without artifacts or with required sensitivity. To improve the image quality, one employs a powerful technique of 'self calibration'. Self calibration uses 'phase closure' and 'amplitude closure' relations as constraints to solve for N unknown complex gains for an N element interferometer using the following iterative scheme :

- Choose a model for brightness distribution and compute the model visibilities.
- Solve for the antenna gains for this model using phase and amplitude closure constraints.
- Apply the solved gain corrections to the visibility data. Use the corrected data to create a new model for brightness distribution.
- repeat the above steps iteratively.

3.3.2.5 Flux Measurements

Once the final image is produced, flux densities and associated uncertainties of the desired sources can be estimated using various AIPS tasks such as JMFIT, IMSTAT, TVSTAT.

3.4 X-ray Observations

X-rays with energy > 30 keV can penetrate the air, at least for a distance of a few meters, but lower energy x-ray photons can not. The x-rays in the 0.5 – 5 keV range, where most celestial sources radiate, can be stopped by a few sheets of paper. Obviously, observations of any astronomical source in the x-rays have to be done

from outside the Earth's atmosphere i.e. to observe x-rays from the sky, the x-ray detectors must be flown above most of the Earth's atmosphere.

Swift [4] (Gehrels et al., 2004), a satellite dedicated for detection and follow-up of GRBs was launched by NASA in November 2004. Till date *Swift* has detected more than 200 GRBs and their afterglows. *XMM-Newton* and *Chandra* are also other satellites which have done follow-up observations of a number of GRB afterglows at various times. Since we have analysed and used data only from *Swift*, we will briefly discuss it in this chapter.

The prime goal of *Swift* is the detection and quick follow-up of GRBs and afterglows. *Swift* carries three major instruments aboard : [1] Burst Alert Telescope (BAT) which operates in the energy range $15-150$ keV. BAT detects the GRBs and immediately slews towards the GRB for follow-up in x-ray and optical bands. [2] Ultra-violet and optical Telescope (UVOT) which operates in the waveband $170-650$ nm. UVOT is not only useful for quick optical follow-up but also for refining the positions of the afterglows. [3] X-ray Telescope (XRT) which operates in the $0.3-10$ keV energy range. The XRT can pinpoint GRBs to $5''$ accuracy and can study the x-ray counterparts of GRBs – beginning within a few tens of seconds and continuing for days to weeks. The XRT also has a wide dynamic range covering more than 7 orders of magnitudes in flux. In the following sections we briefly describe the XRT specifications and related data analysis techniques.

3.4.1 Telescope

3.4.1.1 XRT Modes

The XRT can operate in two states : Manual and Auto. The manual state is used for calibration purposes whereas the auto state is used for automatic controlling of

[4] http://swift.gsfc.nasa.gov/docs/swift/swiftsc.html

Telescope:	Wolter I (3.5 m focal length)
Detector:	E2V CCD-22
Pixel Size:	40μ m $\times$ 40μ m
Pixel Scale :	2.36 arcsec per pixel
Field of View :	23.6×23.6 arcmin
PSF:	18 arcsec HPD at 1.5 keV
	22 arcsec HPD at 8.1 keV
Position accuracy :	3 arcsec
Energy Range :	0.2-10 keV
Energy Resolution:	140 eV at 5.9 keV (at launch)
Effective Area:	135 cm^2 at 1.5 keV
	20 cm^2 at 8.1 keV
Sensitivity :	2×10^{-14} erg cm^{-2} s^{-1} at 104 sec
	in Photon Counting mode
	(about 2μ Crab)

Table 3.5: **XRT Characteristics :** This table is taken from 'The SWIFT XRT Data Reduction Guide' by Capalbi et al. (2005). This guide can be downloaded from "http://swift.gsfc.nasa.gov/docs/swift/analysis/"

the observations and selection of various modes depending on the count rate. The XRT can operate in following four science modes :

- Image mode : When a new GRB is detected the XRT switches to this mode and stores an image of the source to calculate the source position. The time resolution of this mode is automatically set to 0.1 or 2.5 s depending on the source brightness. The image mode is useful for fluxes between 25 mCrab and 45 Crab.

- Low Rate and Piled-up Photodiode mode : This is designed for very bright sources and for high time resolution. This mode does not have any spatial information. The time resolution of this mode is 0.14 ms. These modes are

useful for fluxes up to 60 Crab.

- Windowed Timing : This is obtained by binning 10 rows into a single row and then reading out only the central 200 columns of the CCD. It thus covers the central 8 arcmin of the field of view and can do one dimensional imaging. The time resolution of this mode is 1.7 ms. This mode is useful for fluxes between 1-600 mCrab.

- Photon Counting : This mode retains full imaging and spectroscopic resolution but the time resolution is limited (2.5 s). This mode is useful for fluxes below 1 mCrab and is piled-up if there are more than 2 source counts per frame.

3.4.1.2 Classification of Events and Grades

Based on distribution of charge, x-ray events are classified into different grades. For the Photon Counting mode the events are classified into 32 grades and those for the Windowed Timing into 15 different grades. For details of this classification see Capalbi et al. (2005)

For the Photon counting mode, grades in the range of 0-12 are considered good grades. Similarly, for the Windowed Timing and Photodiode modes, the grades in the range 0-2 and 0-5, respectively, are considered good.

3.4.1.3 Calibration Data Base

The software interfaces with the calibration information via the Calibration Database (CALDB). CALDB consists of a collection of files, each dedicated to a specific aspect of the calibration, organized in a specific directory structure. Along with other files it includes the files which are used in the analysis of the extracted products, for example, the response matrices : Response Matrix File (RMF) and Ancillary Response File (ARF). The RMF files are provided through the XRT CALDB

and the ARFs can be created using task XRTMKARF.

- **RMF :** The RMF files contain information about the channel distribution of photons.

- **ARF :** The ARF files contain information about the telescope area and efficiency as function of energy.

The complete list of XRT calibration files and their format are described in a separate document, "Description of the XRT Calibration Files", available at *http : //heasarc.gsfc.nasa.gov/docs/caldb/swift/*

3.4.2 Data Reduction and Analysis

3.4.2.1 XRT Pipeline

The data files which are provided by the *Swift* archive are clean (bad pixels identified, coordinates transformed, time tagged, piled up frames and partially exposed pixels eliminated), calibrated and screened for various parameters including 'good' grades. However one can start from the raw data files and perform all these operations independently. The best way of doing this is by running a script XRTPIPELINE.

All the above steps have been implemented in the XRTPIPELINE script. The script allows the user to set several parameters, many of which have been already set to a default. XRTPIPELINE assumes that users have downloaded the data from the archive and it searches in the sequence directory for the appropriate input files required to run the individual tasks. Output of the XRTPIPELINE are clean, screened and calibrated event files which can further be processed to get image, spectra and light curves.

3.4.2.2 Extracting Products

The images, spectra and light curves for sources and their backgrounds can be extracted from the clean event files using XSELECT.

We used XSELECT to extract images in WT and PC modes. While extracting the images we selected only those events which had grades between 0-12 for PC mode and 0-2 for WT mode. One can then select a region of different shape and size around the point of interest, generally the source or its background, in the image. For PC mode, we used a circular region of radius 20" centered on the source for extracting its spectrum and light curve. For extracting the spectrum and light curve corresponding to the background we used an annular region, enclosed between the source region and a circle of radius 40" centered on the source. For WT mode, we used a rectangle of size 20×40 pixels. We could thus extract the source spectrum and light curve by placing the rectangle on the source. When placed far away from the source, the same rectangle could be used to extract the spectrum and light curves of the background.

After having extracted the images, spectra and light curves they can be further analysed using various packages such as XSPEC, XRONOS ad XIMAGE.

3.4.2.3 Spectral Model Fitting

XSPEC is a x-ray spectral analysis package that is commonly used for plotting and model fitting. The source and background spectra created in XSELECT are given as input to the XSPEC along with the corresponding Response Matrix File (RMF) and Ancillary Response File (ARF). To improve the statistics we binned the spectrum such that at least 20 counts are collected in each energy bin using a task GRPPHA in XSPEC. The resultant background subtracted spectrum could then plotted in XSPEC. Almost all the afterglows show initially rising spectrum, which

after reaching a peak at ~ 1 keV, declines. We found that the power-law spectrum convolved with some absorption gives a best fit to the afterglow spectra. Therefore, we have used Wilkinson Absorption convolved with the Power Law spectrum – wabs × powerlaw – as a model to fit the observed spectra and to determine various parameters such as neutral hydrogen column density (N_H), index of the power law (spectral photon index) and its normalisation at 1 keV. The best fit values of these parameters for individual afterglows are quoted in different chapters of this thesis. These best fit parameters are also useful for converting the count-rate into erg s^{-1} cm^{-2} Hz^{-1} (or Jansky units) which are finally used for modeling the multi-frequency data sets.

3.4.2.4 Analysis of light curves

The light curves obtained by using XSELECT can be further analysed using various simple tasks like LCURVE, LCMATH etc. We used a task LCMATH to subtract the background light curve from the combined light curve of source and background. The task LCMATH allows to weight the individual light curves according to the area of the corresponding region used before subtracting. The source light curve thus obtained can be plotted and re-binned using another task LCURVE. Finally a suitably binned light curve thus obtained is in the units *counts* s^{-1}. To convert to Jansky units one has to take into account the spectrum of the afterglow. Consider a power law photon spectrum

$$\frac{d\dot{N}}{dE} = \dot{N}_0 \left(\frac{E}{E_0}\right)^{-\alpha} \tag{3.7}$$

which extends from lower energy E_1 to higher energy E_2 with $\dot{N}$ being the *counts* s^{-1}, $\dot{N}_0$ the *counts* s^{-1} at the energy of normalisation E_0 and α the index of power law called as the 'Photon Index'. E is the energy of interest at which one wishes to calculate further quantities such as a light curve. The spectral fitting in XSPEC

gives the quantity on the left hand side of this equation viz. $counts\ s^{-1}keV^{-1}$. This photon spectrum results in the energy spectrum which can be written as

$$F = F_0 \left(\frac{E}{E_0}\right)^{-\beta} \tag{3.8}$$

where β is the spectral index related to α through $\beta = \alpha - 1$. Using these, one can calculate the flux F_E at any energy E in terms of $\dot{n}$ which is the quantity one obtains after having run LCURVE. This conversion relation can be shown to be

$$F_E = \frac{E_0}{E/h}\ \frac{\dot{n}}{Area}\ \frac{(1-\alpha)}{[x_2^{(1-\alpha)} - x_1^{(1-\alpha)}]} \tag{3.9}$$

The quantity E/h converts the desired energy into equivalent frequency where h is the Planck's constant. $Area$ is the effective area of the telescope at energy E. The quantities x_2 and x_1 are abbreviated notations for (E_2/E_0) and (E_1/E_0), respectively. The fractional error on F_E is estimated by adding in quadrature the fractional errors on the rest of the measured quantities.

$$\left(\frac{\delta F_E}{F_E}\right)^2 = \left(\frac{\delta \dot{n}}{\dot{n}}\right)^2 + \left(\frac{\delta(1-\alpha)}{(1-\alpha)}\right)^2 + \left(\frac{\delta[x_2^{(1-\alpha)} - x_1^{(1-\alpha)}]}{[x_2^{(1-\alpha)} - x_1^{(1-\alpha)}]}\right)^2 \tag{3.10}$$

where the quantities with δ represent errors in the corresponding quantities.

3.5 Summary

To summarize, in this Chapter we have described the telescopes, filter systems and the detectors that we have used for optical, radio and x-ray observations of GRB afterglows. We have discussed in detail the techniques and methods we have followed for observations and subsequent data reduction and analysis.

Bibliography

Baars J.W.M., Genzel R., Pauliny-Toth I.I.K. and Witzel A. A&A, 61, 99 (1977).

Capalbi M., Perri M., Saija B., Tamburell F. and Angelini L. (2005).

de Ugarte Postigo A., Fatkhullin T.A., Jóhannesson G. et al. A&A, 462, L57 (2007).

Gehrels N., Chincarini G., Giommi P. et al. ApJ, 611, 1005 (2004).

Henden A.A. and Kaitchuck R.H. Astronomical photometry (New York, Van Nostrand Reinhold Co., 1982. 405 p., 1982).

Ishwara-Chandra C.H., Kamble A.P. and Resmi L. GRB Coordinates Network, 3369, 1 (2005).

Kamble A., Ishwara-Chandra C.H. and Bhattacharya D. GRB Coordinates Network, 3861, 1 (2005).

Kamble A., Ishwara-Chandra C.H. and Bhattacharya D. GRB Coordinates Network, 4840, 1 (2006a).

Kamble A., Ishwara-Chandra C.H. and Bhattacharya D. GRB Coordinates Network, 4832, 1 (2006b).

Landolt A.U. AJ, 104, 340 (1992).

Ryle M. and Hewish A. MNRAS, 120, 220 (1960).

Stetson P.B. PASP, 99, 191 (1987).

Swarup G. Indian Journal of Radio and Space Physics, 19, 493 (1990).

Taylor G.B., Carilli C.L. and Perley R.A., (Eds.). Synthesis Imaging in Radio Astronomy II, volume 180 of Astronomical Society of the Pacific Conference Series (1999).

van der Horst A.J., Kamble A., Resmi L. et al. ArXiv e-prints, 706 (2007).